Preprints of the 21st IFAC World Congress (Virtual)
Berlin, Germany, July 12-17, 2020

Magnetometer-free inertial motion tracking of arbitrary joints with range of motion constraints

Dustin Lehmann * **Daniel Laidig** ** **Raphael Deimel** ***
Thomas Seel ****

* *Technische Universität Berlin, Control Systems Group (e-mail: dustin.lehmann@tu-berlin.de).*
** *Technische Universität Berlin, Control Systems Group (e-mail: laidig@control.tu-berlin.de)*
*** *Technische Universität Berlin (e-mail: raphael.deimel@tu-berlin.de)*
**** *Technische Universität Berlin, Control Systems Group (e-mail: seel@control.tu-berlin.de)*

Abstract: In motion tracking of connected multi-body systems, Inertial Measurement Units (IMUs) are used in a wide variety of applications, since they provide a low-cost easy-to-use method for orientation estimation. However, in indoor environments or near ferromagnetic material, the magnetic field is inhomogeneous, which limits the accuracy of tracking algorithms using magnetometers. Methods that use only accelerometers and gyroscopes on the other hand yield no information on the absolute heading of the tracked object. For objects connected by rotational joints with range of motion constraints, a method is proposed that provides a magnetometer-free, long-term stable relative orientation estimate based on a non-linear, window-based cost function. The method can be used for real-time estimation as well as post-processing. It is validated experimentally with a mechanical joint and compared to other methods that are commonly used in motion tracking. It is shown that for the used test object, the proposed method yields the best results with a total angle error of less than 4° for all experiments.

Keywords: information and sensor fusion, inertial measurement units, inertial sensors, motion tracking, state estimation, magnetometer-free inertial motion tracking, exploitation of kinematic constraints, moving horizon estimation

1. INTRODUCTION

The tracking of orientations and positions of objects in three-dimensional space is an integral part of various control applications. Many mechanical systems consist of multiple connected objects of which the individual orientations must be known for a specific control task to be feasible. There exist numerous different approaches for orientation tracking reaching from optical systems over mechanical solutions to inertial sensors. In contrast to other solutions, microelectromechanical systems (MEMS)-based inertial Measurement Units (IMUs) have the advantage of being small, low-cost, having a wide field of application and not requiring neither direct interaction with the object of interest nor a clear line of sight. Therefore, they are used in a wide variety of robotic and biomedical applications (Wong et al., 2015; Miller et al., 2004; Fong and Chan, 2010).

IMUs typically consist of 3D accelerometers, 3D gyroscopes and 3D magnetometers. Sensor fusion of the measurements yields the orientation of the sensor with respect to an inertial reference frame that neither rotates nor accelerates. This common inertial frame is necessary to determine the relationships between the individual segments of a kinematic chain. However, 9D sensor fusion only yields accurate orientation estimates if the magnetic field is homogeneous. In indoor environments and near ferromagnetic material, the magnetic field is known to be highly disturbed and inhomogeneous (Subbu et al., 2013; de Vries et al., 2009; Shu et al., 2015; Grand and Thrun, 2012). This is relevant for most robotic and biomedical applications and makes conventional 9D sensor fusion inapplicable (Salchow-Hömmen et al., 2019). Without magnetometers, the heading component of the orientation is unknown. While the inclination of individual bodies can still be determined with high accuracy (Seel et al., 2015), the estimated orientations of connected segments cannot be used to determine relative orientations, joint angles or positional relationships.

One approach to solve this problem is to omit the magnetometer readings and determine the heading by predefined initial poses. It has been shown that this leads to better results than conventional 9D sensor fusion (Salchow-Hömmen et al., 2019). However, due to non-zero residual bias and integration drift, this method only produces good results for short-term experiments ($< 30\,\mathrm{s}$) and is not long-term stable. Therefore, current research aims at exploiting the kinematic relationships between the connected bodies to obtain heading information without using magnetometers or predefined initial poses.

For joints with one degree of freedom there exist methods to calculate the joint angles analytically without the use of magnetometers (Cooper et al., 2009; Seel et al., 2014). Recently a method was published which exploits the kinematic relationships with an orientation-based constraint (Laidig et al., 2017a) to estimate the relative heading of two bodies connected by a one-dimensional joint.

For joints with two degrees of freedom, we recently proposed an orientation-based constraint that is independent of excitation and raw measurement data (Laidig et al., 2019). One drawback of such methods is that they require joint kinematics with limited degrees of freedom as well as known joint axes and sensor-to-segment calibration (Olsson et al., 2019; Laidig et al., 2017b). If these requirements are met, such methods can produce accurate results by exploiting the limited degrees of freedom to formulate kinematic constraints.

For three-dimensional joints, Kok et al. (2014) and Taetz et al. (2016) exploit positional relationships and use those to estimate the true relative orientations of connected bodies. However, they still rely on magnetometers for the initialization. In Wenk and Frese (2015) an approach is proposed that uses an extended Kalman filter (EKF) to estimate the orientation of two bodies connected by a ball joint. It is based on the knowledge of the relative position of the IMUs with respect to the joint center. These approaches for three-dimensional joints have in common that they rely on positional constraints and relationships or use magnetometer data for initial heading estimation.

In the present paper, a magnetometer-free method is proposed that works for relative motion tracking of kinematic chains with arbitrary joints that have limited range of motion (ROM). The method will be applicable to any rotational (1D, 2D and 3D) joints with ROM constraints and is only based on the orientations of the objects. It further does not need any knowledge on initial orientation or positions of the IMUs and yields a long-term stable estimation even under realistic conditions. The proposed method shows remarkable similarities to a moving horizon estimation (MHE) and can be formulated as such.

2. KINEMATICS AND GENERIC JOINT MODEL

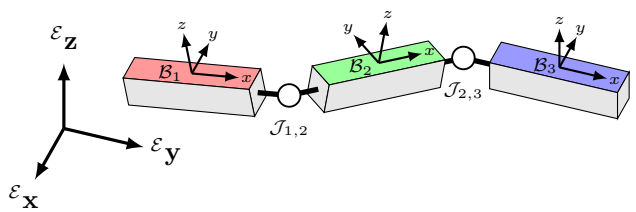

Fig. 1. Model of a kinematic chain consisting of segments $\mathcal{B}$ connected by joints $\mathcal{J}$

Consider a system of N segments connected by $N-1$ joints. Segments are denoted $\mathcal{B}_\mathrm{i}$, $i \in [1, N]$. The joint connecting the segments $\mathcal{B}_\mathrm{i}$ and $\mathcal{B}_{\mathrm{i}+1}$ is denoted as $\mathcal{J}_{\mathrm{i},\mathrm{i}+1}$. Joints connect only two adjacent segments to form a kinematic pair. An example for this system is shown in Fig. 1. Only rotational joints are considered which allow for relative rotations of the two connected segments with respect to each other. The orientation of each segment with respect to a reference frame is expressed by a quaternion. The common reference for all segments is denoted by $\mathcal{E}$. The orientation of $\mathcal{B}_\mathrm{i}$ with respect to $\mathcal{E}$ is denoted as ${}^{\mathcal{B}_\mathrm{i}}_{\mathcal{E}}\mathbf{q}$. The relative orientation ${}^{\mathcal{B}_{\mathrm{i}+1}}_{\mathcal{B}_\mathrm{i}}\mathbf{q}$ of two adjacent segments $\mathcal{B}_\mathrm{i}$ and $\mathcal{B}_{\mathrm{i}+1}$ describes the orientation of $\mathcal{B}_{\mathrm{i}+1}$ with respect to the coordinate system of $\mathcal{B}_\mathrm{i}$ and can be determined from the orientations of both segments in the common reference frame:

$$ {}^{\mathcal{B}_{\mathrm{i}+1}}_{\mathcal{B}_\mathrm{i}}\mathbf{q} = {}^{\mathcal{B}_\mathrm{i}}_{\mathcal{E}}\mathbf{q}^{-1} \otimes {}^{\mathcal{B}_{\mathrm{i}+1}}_{\mathcal{E}}\mathbf{q}. \tag{1} $$

The relative orientation of the two segments is caused by the rotation around the joint connecting the two segments. A joint can either allow free relative rotation of the segments, or the space of possible relative orientations of those segments is restricted. These restrictions can either be due to limited degrees of freedom (one- and two-dimensional joints), due to limitations of the range of motion or due to both. If the joint $\mathcal{J}_{\mathrm{i},\mathrm{i}+1}$ has restrictions of degrees of freedom or range of motion, the set of possible relative orientations ${}^{\mathcal{B}_{\mathrm{i}+1}}_{\mathcal{B}_\mathrm{i}}\mathbf{q}$ of the two adjacent segments is limited to a subset of all possible orientations $\mathbb{H}$. This subset is denoted as P with

$$ \mathrm{P} \subseteq \mathbb{H}. \tag{2} $$

To describe the relative orientation of the two connected segments, a generic joint model based on the concept of *joint axes* is proposed. The rotation ${}^{\mathcal{B}_{\mathrm{i}+1}}_{\mathcal{B}_\mathrm{i}}\mathbf{q}$ from $\mathcal{B}_\mathrm{i}$ to $\mathcal{B}_{\mathrm{i}+1}$ is modeled as consecutive rotations around the joint axes $\boldsymbol{j}_\mathrm{p} \in \mathbb{R}^3$, $\|\boldsymbol{j}_\mathrm{p}\| = 1$, by the *joint angles* $\varphi_\mathrm{p} \in \mathbb{R}$, $\mathrm{p} \in [1 \dots 3]$. The restriction of the relative orientation is modeled as limitations of the range of motion of one or more joint angles with

$$ \varphi_\mathrm{p} \in \{\varphi \in \mathbb{R} | \varphi_{\mathrm{p,min}} \leq \varphi \leq \varphi_{\mathrm{p,max}}\}. \tag{3} $$

The relative orientation is then modeled as consecutive rotations around the joint axes

$$ {}^{\mathcal{B}_{\mathrm{i}+1}}_{\mathcal{B}_\mathrm{i}}\mathbf{q} = \mathrm{Q}(\varphi_1, \boldsymbol{j}_1) \otimes \mathrm{Q}(\varphi_2, \boldsymbol{j}_2) \otimes \mathrm{Q}(\varphi_3, \boldsymbol{j}_3) = \prod_{p=1}^{3} \mathrm{Q}(\varphi_\mathrm{p}, \boldsymbol{j}_\mathrm{p}) . \tag{4} $$

The operator $\mathrm{Q}(\alpha, \boldsymbol{j})$ denotes the quaternion that represents the rotation of α around the axis $\boldsymbol{j}$. The operator $\otimes$ denotes quaternion multiplication.

This model can describe most types of rotational joints. For one- and two-dimensional joints, the predefined joint axes are chosen as $\boldsymbol{j}_\mathrm{p}$. For the remaining, restricted degrees of freedom, linearly independent axes are chosen with a fixed value for the corresponding joint angle, i.e.

$$ \varphi_{\mathrm{p,min}} = \varphi_{\mathrm{p,max}}. \tag{5} $$

This limits the relative orientation to rotations around the predefined joint axes of those joints. For three-dimensional joints, the joint axes $\boldsymbol{j}_\mathrm{p}$ are chosen either as the predefined axes if the joint is a serial composition of hinge joints (see Fig. 2 left) or can be chosen freely for joints with no distinct axes (see Fig. 2 right). The set which contains all orientations described by the model (4) is denoted as $\mathrm{P_M}$ and is defined as

$$ \mathrm{P_M} := \left\{ \mathbf{q} \in \mathbb{H} \,\middle|\, \mathbf{q} = \prod_{\mathrm{p}=1}^{3} \mathrm{Q}(\varphi_\mathrm{p}, \boldsymbol{j}_\mathrm{p}), \varphi_\mathrm{p} \in [\varphi_{\mathrm{p,min}}, \varphi_{\mathrm{p,max}}] \right\}. \tag{6} $$

The range of each joint angle follows from the mechanical model of the joint or from identification experiments.

Without loss of generality the focus is on the description of joints with three degrees of freedom since they describe the most general case. In Fig. 2 two examples for joints with three degrees of freedom are shown. For the left example

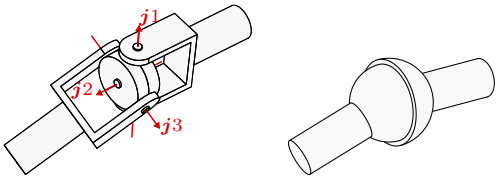

(a) Distinct joint axes for a three-dimensional joint

(b) Ball joint

Fig. 2. Two joints with $\mathrm{dof}(\mathcal{J}) = 3$

(a), the joint axes $\boldsymbol{j}_\mathrm{p}$ and the limits for the joint angles φ_p can be directly extracted from the mechanical model. If the model from (4) is applied to this, it can be seen that $\mathrm{P_M}$ perfectly describes the set of possible relative orientations, therefore $\mathrm{P} = \mathrm{P_M}$. For the three-dimensional ball joint (b) any triplet of linearly independent joint axes can be chosen for the joint model. If the three axes $\boldsymbol{a}, \boldsymbol{b}$ and $\boldsymbol{c}$ are chosen to form an orthonormal base of a right-handed coordinate system, the rotation around the joint can be described by using Euler angles. This is a common approach and is simpler than choosing non-orthogonal axes. The corresponding Euler angles are denoted as $\alpha, \beta, \gamma \in \mathbb{R}$. The limits of the Euler angles describe the range of motion constraints of the joint with

$$\alpha \in [\alpha_\mathrm{min}, \alpha_\mathrm{max}], \beta \in [\beta_\mathrm{min}, \beta_\mathrm{max}], \gamma \in [\gamma_\mathrm{min}, \gamma_\mathrm{max}]\,. \quad (7)$$

If the joint model is applied to this, with $\boldsymbol{a}$, $\boldsymbol{b}$ and $\boldsymbol{c}$ being chosen as the joint axes $\boldsymbol{j}_\mathrm{p}$ and α, β, γ describing the joint angles φ_p, the set described by (6) is a conservative approximation of P since the joint model assumes fixed ranges for all joint angles. This creates a cuboid subspace in the space created by the three joint angles. For the ball joint however, not the complete subspace can be reached. Therefore, for this joint (and all joints in general)

$$\mathrm{P} \subseteq \mathrm{P_M} \subseteq \mathbb{H}\,. \quad (8)$$

Describing each joint with a set of orthogonal axes and Euler angles can be easily applied to most types of rotational joints, which have no distinct joint axes.

In the following derivation we only focus on a single kinematic pair of a kinematic chain with N segments. The proposed method can then be applied to each joint which fulfills the assumptions to estimate the orientations of the complete kinematic chain. Each joint estimation is independent from the other joints in the chain.

3. INERTIAL STATE ESTIMATION

Consider two segments $\mathcal{B}_1$ and $\mathcal{B}_2$ connected by the three-dimensional joint $\mathcal{J}_{1,2}$ with range of motion constraints. To estimate the orientations of the segments with respect to a reference frame, two inertial sensors $\mathcal{S}_1$ and $\mathcal{S}_2$ are placed on the segments in a known and fixed orientation (see Fig. 3). The sensors measure the angular rates $\boldsymbol{\omega}_1(t)$ and $\boldsymbol{\omega}_2(t)$ as well as the accelerations $\mathbf{a}_1(t)$ and $\mathbf{a}_2(t)$ in local coordinates of the sensors with a fixed sampling time T_s. For each segment, 6D quaternion-based sensor fusion is performed (for example according to the algorithm described in Seel and Ruppin (2017)) to obtain the

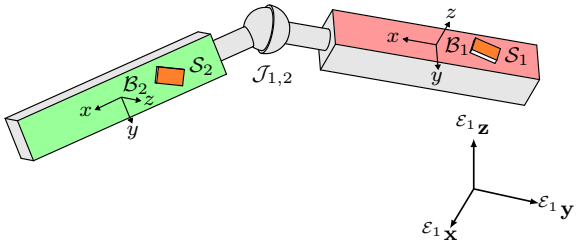

Fig. 3. Kinematic model of two adjacent segments $\mathcal{B}_1$ and $\mathcal{B}_2$ connected by the joint $\mathcal{J}_{1,2}$ and the reference frame $\mathcal{E}_1$

orientation of each segment with respect to a reference frame, i.e. ${}^{\mathcal{B}_1}_{\mathcal{E}_1}\mathbf{q}(t)$ and ${}^{\mathcal{B}_2}_{\mathcal{E}_2}\mathbf{q}(t)$. However, due to the fact that no magnetometer is used and the resulting lack of heading information, the absolute heading of each segment at the beginning of the measurement is arbitrary and only dependent on the initial conditions of the sensor fusion algorithm. This can be modeled as if the orientations of the segments are estimated in different reference frames $\mathcal{E}_1$ and $\mathcal{E}_2$. Since only the heading of each segment is unknown, the difference between the two reference frames $\mathcal{E}_1$ and $\mathcal{E}_2$ can be described by a rotation around the global vertical axis (see Fig. 4). The angle of this rotation is denoted as δ and is called *heading offset* (Laidig et al., 2017a). The rotation from $\mathcal{E}_1$ to $\mathcal{E}_2$ is described by the quaternion

$${}^{\mathcal{E}_2}_{\mathcal{E}_1}\mathbf{q}(\delta) = \left[\cos\left(\tfrac{\delta}{2}\right)\ 0\ 0\ \sin\left(\tfrac{\delta}{2}\right)\right]^T\,. \quad (9)$$

With the two estimated orientations ${}^{\mathcal{B}_1}_{\mathcal{E}_1}\mathbf{q}(t)$ and ${}^{\mathcal{B}_2}_{\mathcal{E}_2}\mathbf{q}(t)$

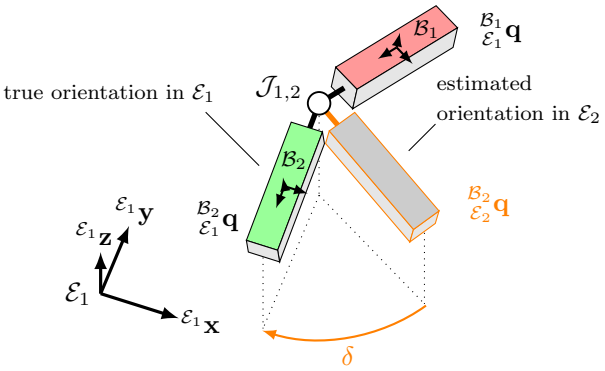

Fig. 4. Difference between the two reference frames $\mathcal{E}_1$ and $\mathcal{E}_2$

and a known value of the heading offset δ, the relative orientation of the two segments can be determined by

$${}^{\mathcal{B}_2}_{\mathcal{B}_1}\mathbf{q}(t) = {}^{\mathcal{B}_1}_{\mathcal{E}_1}\mathbf{q}(t)^{-1} \otimes {}^{\mathcal{E}_2}_{\mathcal{E}_1}\mathbf{q}(\delta) \otimes {}^{\mathcal{B}_2}_{\mathcal{E}_2}\mathbf{q}(t)\,. \quad (10)$$

Due to bias in the gyroscope measurements and the resulting drift around the global vertical axis, the angle δ is not constant and can be approximated as

$$\delta(t) \approx \underbrace{\frac{\partial \delta}{\partial t} \cdot t}_{\text{heading drift}} + \underbrace{\delta(t=0)}_{\text{initial offset } \delta_0}\,. \quad (11)$$

$\frac{\partial \delta}{\partial t}$ is a scalar which is slowly changing due to bias instability and non-uniformity of the bias of each axis. For short time windows the heading offset $\delta(t)$ can be approximated as constant, since the drift is typically small with magnitudes of $\frac{\partial \delta}{\partial t} < 0.5\,\frac{^\circ}{\mathrm{s}}$. Note that no other assumptions on the course of $\delta(t)$ are made.

4. CONSTRAINT

Consider two segments $\mathcal{B}_1$ and $\mathcal{B}_2$ connected by the joint $\mathcal{J}$ with the most general case of three degrees of freedom. The joint has mechanical restrictions which limits the set of possible relative orientations to $\mathrm{P} \subset \mathbb{H}$. The kinematics of the joint are described by an Euler angle convention with the orthonormal axes $\boldsymbol{a}$, $\boldsymbol{b}$ and $\boldsymbol{c}$ and the corresponding angles α, β, γ, which are restricted according to (7). The set of relative orientations described by this model is $\mathrm{P_M}$ with $\mathrm{P} \subseteq \mathrm{P_M}$. At any given point in time t_k, the orientations of the two segments estimated by the 6D sensor fusion are ${}^{\mathcal{B}_1}_{\mathcal{E}_1}\mathbf{q}(t_k)$ and ${}^{\mathcal{B}_2}_{\mathcal{E}_2}\mathbf{q}(t_k)$. The heading offset at that time instant is $\delta(t_k)$. Let $\hat{\delta}$ be an estimate of $\delta(t_k)$, then an estimate ${}^{\mathcal{B}_2}_{\mathcal{B}_1}\hat{\mathbf{q}}$ of the relative orientation can be obtained by

$$ {}^{\mathcal{B}_2}_{\mathcal{B}_1}\hat{\mathbf{q}}(t_k, \hat{\delta}) := {}^{\mathcal{B}_1}_{\mathcal{E}_1}\mathbf{q}(t_k)^{-1} \otimes {}^{\mathcal{E}_2}_{\mathcal{E}_1}\hat{\mathbf{q}}(\hat{\delta}) \otimes {}^{\mathcal{B}_2}_{\mathcal{E}_2}\mathbf{q}(t_k)\,. \tag{12} $$

Let $E_{\mathrm{abc}} : \mathbb{H} \mapsto \mathbb{R}^3$ be an operator that maps any given quaternion $\mathbf{q}$ to a triplet of Euler angles (α, β, γ) according to the intrinsic Euler angles convention a-b'-c'' (Diebel, 2006). To check whether ${}^{\mathcal{B}_2}_{\mathcal{B}_1}\hat{\mathbf{q}}(t_k, \hat{\delta})$ is an element of $\mathrm{P_M}$ at a given time instant t_k and a given estimate $\hat{\delta}$, it has to be decomposed into the Euler angles $\hat{\alpha}$, $\hat{\beta}$ and $\hat{\gamma}$ that correspond to the Euler angle convention a-b'-c''

$$ (\hat{\alpha}, \hat{\beta}, \hat{\gamma}) = E_{\mathrm{abc}}\left({}^{\mathcal{B}_2}_{\mathcal{B}_1}\hat{\mathbf{q}}(t_k, \hat{\delta})\right)\,. \tag{13} $$

If $\hat{\alpha}$, $\hat{\beta}$ and $\hat{\gamma}$ are within the specified ranges according to (7), then it is a valid relative orientation ${}^{\mathcal{B}_2}_{\mathcal{B}_1}\hat{\mathbf{q}}(t_k, \hat{\delta}) \in \mathrm{P_M}$ according to the model. A function $e_k(\hat{\delta}) : \mathbb{R} \mapsto \mathbb{N}$ is defined that assigns a binary value 0 or 1 to an estimate $\hat{\delta}$ at a given time instant t_k with

$$ e_k(\hat{\delta}) := \begin{cases} 0, & \text{if } {}^{\mathcal{B}_2}_{\mathcal{B}_1}\hat{\mathbf{q}}(t_k, \hat{\delta}) \in \mathrm{P_M} \\ 1, & \text{otherwise.} \end{cases} \tag{14} $$

If the three Euler angles for a given $\hat{\delta}$ are within the ranges defined by the model, then $e_k(\hat{\delta}) = 0$ and the orientation is a valid relative orientation for the given joint model.

5. ESTIMATION PRINCIPLE

The basic idea of the estimation of $\delta(t)$ is that at each time instant t_k only a subset of possible values of $\hat{\delta}$ produces a relative orientation ${}^{\mathcal{B}_2}_{\mathcal{B}_1}\hat{\mathbf{q}}(t_k, \hat{\delta})$ according to (12) that lies within the set of possible relative orientations $\mathrm{P_M}$. With the assumption that $\delta(t)$ can be approximated constant over a short time window and the assumption of sufficiently rich motion, only one value of $\hat{\delta}$ produces valid relative orientations for all time instants of that time window, i.e. does not violate the constraint. Therefore, a window-based approach is used to find a good estimate of $\delta(t)$ for a given time interval T_{w}.

At regular time intervals $T_{\mathrm{est}} \geq T_{\mathrm{s}}$, an estimation of $\delta(t)$ is performed at the time instants t_w, which are denoted with an index $w \in \mathbb{N}^+$ and are defined as

$$ t_w := w T_{\mathrm{est}}\,. \tag{15} $$

The number of samples within a window is denoted N_{w}, with samples taken with an interval T_{s} at the sampling instants t_k. The time instants that correspond to a time window w can be determined by

$$ t_k = t_w + (m - N_{\mathrm{w}})T_{\mathrm{s}},\ \ m \in [1 \ldots N_{\mathrm{w}}]\,. \tag{16} $$

To create overlapping time windows, $T_{\mathrm{est}} < T_{\mathrm{w}}$ is chosen. The definition of the time window only incorporates samples that lie before the current estimation time instant, making the method real-time capable.

It is assumed that for sufficiently short time windows the heading offset $\delta(t)$ can be approximated as constant. The constant estimate for the heading offset for a given time window w is denoted by $\hat{\delta}_w$. Following this assumption and the model of $\delta(t)$ from (11), it is assumed that from one time window to the next one the value $\hat{\delta}_w$ does not change rapidly and is close to the previous value $\hat{\delta}_{w-1}$. A cost function $c_w(\hat{\delta}) : \mathbb{R} \mapsto \mathbb{R}$ is defined that for a given time window w assigns a cost to a value of $\hat{\delta}$ with

$$ c_w(\hat{\delta}) := \frac{N_w}{\pi}|(\hat{\delta} - \hat{\delta}_{w-1})| + \sum_{m=1}^{N_w} e_k(\hat{\delta})\,, \tag{17} $$

with $k = w\frac{T_{\mathrm{est}}}{T_{\mathrm{s}}} + (m - N_w)$.

The first term penalizes the distance from the previous estimate $\hat{\delta}_{w-1}$. This ensures that the new estimate $\hat{\delta}_w$ is close to the previous estimate. The scaling factor $\frac{N_w}{\pi}$ scales the cost so that a distance of π is equal to the maximum cost of the second term. Note that this only penalizes the distance and does not make assumptions on the direction of change. The second term is a measure of how well the estimate $\hat{\delta}$ fulfills the kinematic constraint. The more valid relative orientations $\hat{\delta}$ produces over the time window, the smaller the second term gets. The cost function (17) is then used to find an estimate $\hat{\delta}_w$ for a time window that minimizes the cost over that window by the help of any optimization method, i.e.

$$ \hat{\delta}_w := \arg\min_{\hat{\delta}} c_w(\hat{\delta})\,. \tag{18} $$

Note that the proposed method can be interpreted as a moving horizon estimation approach for a dynamical system with one state δ, which has an uncertain but small time derivative, and a highly non-linear output (14), which we know to be zero up to small inaccuracies. The cost function (17) penalizes outputs different from these virtual zero measurements as well as state values that disagree with the uncertain dynamics.

For any time instant t_k the value of the estimated heading offset $\hat{\delta}(t_k)$ can be determined with

$$ \hat{\delta}(t_k) = \hat{\delta}_{\tilde{w}} \quad \text{with} \quad \tilde{w} = \left\lfloor \frac{k}{N_{\mathrm{w}}} \right\rfloor \in \mathbb{N}^+\,. \tag{19} $$

In Fig. 5 three examples for possible cost function values $c_w(\hat{\delta})$ over $\hat{\delta} \in [0, 2\pi]$ are shown. In the left graph, the constraint part of the cost function dominates. In the right graph, the distance cost to the previous estimate has more impact and ensures a non-diverging estimate even if the constraint minimum is less distinct. With an estimate $\hat{\delta}(t)$, both estimated orientations ${}^{\mathcal{B}_1}_{\mathcal{E}_1}\mathbf{q}(t)$ and ${}^{\mathcal{B}_2}_{\mathcal{E}_2}\mathbf{q}(t)$ can be transformed into a common reference frame. This allows us to calculate the relative orientation, joint angles and positional relationships between the connected segments

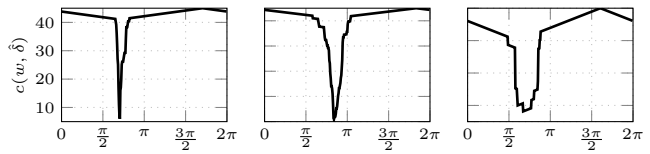

Fig. 5. Examples for cost functions $c_w(\hat{\delta})$ over $\hat{\delta} \in [0, 2\pi]$

or to transform all body orientations of a kinematic chain into one common reference frame.

5.1 Limitations

The main assumptions of the proposed method are that the joints are rotational joints that have a limited range of motion. Furthermore, the restriction in range of motion is assumed to be known. If one of those assumptions is not met, e.g. in biological systems where the joints can only be approximated as rotational joints, the accuracy of the estimation can be reduced. However, even in imperfect rotational joints the method can produce good results. The range of motions can also be determined by identification experiments using a different method.

6. EXPERIMENTAL VALIDATION

The proposed method is validated experimentally with the use of a mechanical three-dimensional joint as a test object. An optical motion capture system is used as a validation method to measure the relative orientation with very high precision. Different motion patterns and speeds are investigated to evaluate the robustness of the method.

6.1 Setup

The test object is 3D printed (see Fig. 6) with a well-defined three-dimensional joint connecting the two segments. To bridge the gap to an application of the method in a biomedical environment, the range of motion of the joint angles is based on the Carpometacarpal joint of the thumb of the author. The joint is modeled by a z-x'-y''

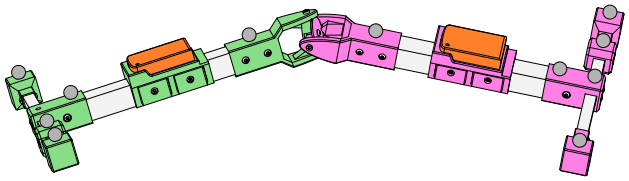

Fig. 6. Mechanical model used for experimental evaluation. The two segments are connected by a well-defined 3D joint. On each segment, IR-reflective markers are attached for optical motion capture.

Euler angles convention with the angle ranges

$$\alpha \in [-20°, 20°], \quad \beta \in [-15°, 15°], \quad \gamma \in [-40°, 40°]. \quad (20)$$

The joint axes $\boldsymbol{j}_1$, $\boldsymbol{j}_2$ and $\boldsymbol{j}_3$ are known and coincide with the axes of the z-x'-y'' Euler rotation sequence. On each segment, an IMU is placed in a known and constant orientation. The IMUs measure the angular velocity and the acceleration of each segment at a rate of 75 Hz and 6D sensor fusion is performed using the algorithm presented in Seel and Ruppin (2017).

6.2 Optical reference

As a ground truth for the relative orientation of the two segments an optical motion capture system (MoCap) is used. It consists of ten *Optitrack Flex 13* cameras, attached in a rectangular pattern at the top of the measurement space. 11 (5+6) IR-reflective markers are attached to the segments in a well-defined and known pattern (see Fig. 6). The MoCap systems determines the 3D positions of the markers at a rate of 120 Hz with a mean position error of less than 0.3 mm. With the marker positions, each segment's orientation can be calculated at each sample time instant in a common reference frame and with (1) the true relative orientation ${}^{\mathcal{B}_2}_{\mathcal{B}_1}\mathbf{q}(t)$ of both segments can be determined.

6.3 Validation metrics

Let ${}^{\mathcal{B}_2}_{\mathcal{B}_1}\hat{\mathbf{q}}(t)$ be the estimated relative orientation of the two segments determined by the algorithm described above. Let ${}^{\mathcal{B}_2}_{\mathcal{B}_1}\mathbf{q}(t)$ be the true relative orientation determined by the MoCap system. The *orientation error* $\epsilon(t)$ is defined to be the error angle between the estimated and true relative orientation, i.e.

$$\epsilon(t) := \left| \mathrm{A}\left({}^{\mathcal{B}_2}_{\mathcal{B}_1}\mathbf{q}(t)^{-1} \otimes {}^{\mathcal{B}_2}_{\mathcal{B}_1}\hat{\mathbf{q}}(t) \right) \right|, \quad (21)$$

with $A(\mathbf{q})$ being the operator that extracts the angle of the corresponding quaternion $\mathbf{q}$. To quantify the method's ability to estimate the heading offset $\delta(t)$, the error $\epsilon_\delta(t)$ is introduced, which is defined as the difference between the true and estimated value of $\delta(t)$

$$\epsilon_\delta := |\delta(t) - \hat{\delta}(t)|. \quad (22)$$

The error $\epsilon_\delta(t)$ is the heading component of $\epsilon(t)$ after being transformed into the global reference frame. To quantify the overall performance over the course of an experiment, the metrics ϵ_{RMS} and $\epsilon_{\delta,\mathrm{RMS}}$ are used, which are the root-mean-square error (RMSE) of their corresponding error metric.

6.4 Conducted experiments

Multiple short-term and long-term experiments have been conducted to test the initial estimation as well as the long-term stability. At the beginning of each experiment, the test object is resting in a random orientation on a table. It is then picked up, rotated and translated within the measurement space of the MoCap system. In all experiments the magnitude and frequency of excitation have been varied. For the estimation a window time $T_\mathrm{w} = 8\,\mathrm{s}$ and an estimation time $T_\mathrm{est} = 1\,\mathrm{s}$ are used. A list of the experiments and their durations is given in Table 1.

Table 1. Performed experiments

Experiment	Duration	Remark
E_01	64 s	random starting orientation
E_02	62 s	random starting orientation
E_03	64 s	random starting orientation
E_04	301 s	fast movement
E_05	212 s	slow movement
E_06	305 s	mixed movement with pauses
E_07	418 s	long measurement

6.5 Results

The method has to fulfill two objectives: 1) converge towards the initial heading offset δ_0 at the beginning of the estimation and therefore the initial relative orientation and 2) track the course of $\delta(t)$ over an arbitrary length of the experiment for long-term stability. In Fig. 7 the error $\epsilon(t)$ for all experiments is shown for the first 10 seconds as well as for the complete experiments. Despite initial errors $> 20°$, the error converges below 5° within 5 s and drops below 4° after $t > 60$ s in all experiments. The mean RMSE for all experiments is $\epsilon_{\text{RMS}} = 2.1°$ with a heading tracking error of $\epsilon_{\delta,\text{RMS}} = 0.8°$. The method can estimate the true relative orientation very fast at the beginning of each estimation, which eradicates the need for predefined initial poses. The method is also able to track the relative orientation with a high accuracy even for long experiments and without external heading correction.

In Fig. 8 the estimation of $\delta(t)$ for one of the experiments is shown in more detail. The estimate $\hat{\delta}$ follows the reference accurately with a mean error of $\epsilon_{\delta,\text{RMS}} = 0.9°$. During the interval $t \in [164\,\text{s}, 184\,\text{s}]$ the test object is lying down with no excitation. During that phase the first term of (17) ensures that the estimate does not diverge and stays close to the true value of $\delta(t)$. For this experiment, the error $\epsilon(t)$ is shown in Fig. 9 for the proposed method with kinematic constraints (KC), 6D sensor fusion without constraints and only initial heading correction and bias compensation (6D) (Salchow-Hömmen et al., 2019) as well as conventional 9D sensor fusion with magnetometer correction (9D). The proposed method performs best, with $\epsilon_{\text{RMS}} = 2.2°$. The 6D method produces adequate results at the beginning of the experiment but due to drift the relative orientation diverges, leading to a maximum error of 34°. Conventional 9D sensor fusion produces temporarily accurate results, but due to magnetic disturbances it has a RMSE of $\epsilon_{\text{RMS}} = 6.8°$ with a maximum error of 18°. The mean and maximum errors for all experiments

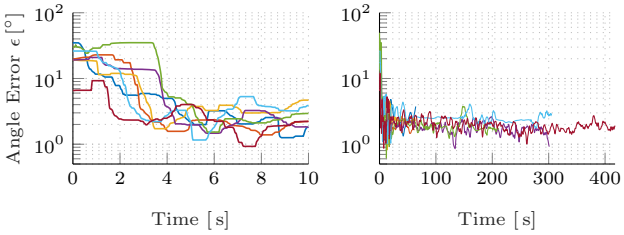

Fig. 7. Error $\epsilon(t)$ for all experiments. Left: initial convergence during the first 10 seconds. Right: Error of the complete experiments.

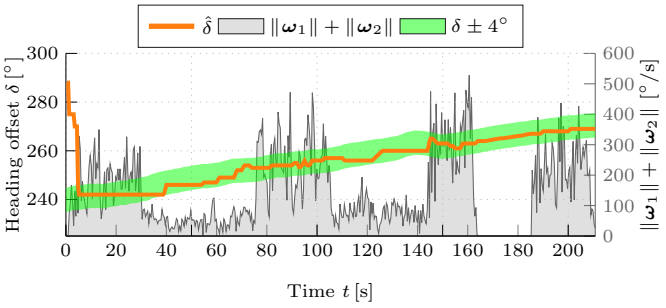

Fig. 8. Estimate $\hat{\delta}(t)$ and reference value $\delta(t)$ for experiment E_05 as well as the norm of gyroscope measurements to indicate excitation. The estimate stays close to the true value $\delta(t)$ even during the phase with no excitation.

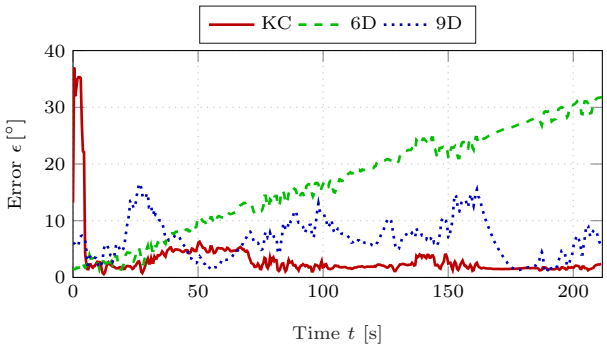

Fig. 9. Errors $\epsilon(t)$ for the three evaluated methods for the experiment E_05. The proposed method (KC) performs significantly better than the other two methods and can maintain a stable orientation estimate even for long-term experiments.

are given in Table 2. Additionally, the results for the conventional 6D and 9D sensor fusion methods are presented. The values in parentheses indicate the maximum errors $\max(\epsilon(t))$ and $\max(\epsilon_\delta(t))$ of all experiments. The proposed method produces the best results with mean orientation errors of $\epsilon_{\text{RMS}} = 2.1°$ and maximum orientation errors of $\max(\epsilon(t)) = 4°$. The main objective of the method to track the heading offset is accomplished with a mean error of less than 1° for all experiments. The two conventional methods produce worse results with mean errors of approx. 6° and maximum errors larger than 20°.

Table 2. Mean error over all experiments and maximum error over all experiments and time instants in parentheses

Error	KC	6D	9D
ϵ_{RMS}	**2.1°** (4°)	6.1° (34°)	6.3° (21°)
$\epsilon_{\delta,\text{RMS}}$	**0.8°** (2°)	5.4° (32°)	5.9° (20°)

7. CONCLUSION

A new method for magnetometer-free inertial motion tracking for arbitrary joints with limited range of motion is proposed. The method exploits range of motion constraints and the resulting limited set of possible relative orientations of two connected segments. From this, the method is used to estimate the relative heading of the two segments using a window-based optimization approach. To apply the method to different joint geometries, a generic joint model is proposed for rotational joints, which can sufficiently approximate joints with no distinct joint axes.

The method enables magnetometer-free real-time tracking in real-world indoor environments. It has been shown in a case study that the proposed method yields a long-term stable estimate. In contrast to other methods that also omit the magnetometer readings, the proposed method does not rely on known initial poses and converges to the true relative orientation within seconds. The performance

of the method is demonstrated experimentally with a mechanical test object. For this experiment the method yields significantly better results than conventional 9D motion tracking and is long-term stable unlike pure 6D motion tracking methods.

However, compared to different orientation-based constraints that exploit the limited degrees of freedom of one- and two-dimensional joints (Laidig et al., 2017a, 2019), the method needs recurrent excitation. Furthermore, the method only works for joints where at least one of the joint angles has a significant range of motion restriction.

Future work aims at overcoming the set limitations, i.e. investigating the sufficiency of rich motion, the magnitude of the angular restrictions as well as validating the method in less rigid, biological joints.

ACKNOWLEDGEMENTS

We gratefully acknowledge financial support for the project MTI-engAge (16SV7109) by BMBF.

REFERENCES

Cooper, G., Sheret, I., McMillian, L., Siliverdis, K., Sha, N., Hodgins, D., Kenney, L., and Howard, D. (2009). Inertial sensor-based knee flexion/extension angle estimation. *Journal of Biomechanics*, 42(16), 2678–2685. doi:10.1016/j.jbiomech.2009.08.004.

de Vries, W.H.K., Veeger, H.E.J., Baten, C.T.M., and van der Helm, F.C.T. (2009). Magnetic distortion in motion labs, implications for validating inertial magnetic sensors. *Gait & Posture*, 29(4), 535–541. doi:10.1016/j.gaitpost.2008.12.004.

Diebel, J. (2006). Representing attitude : Euler angles, unit quaternions, and rotation vectors.

Fong, D.T.P. and Chan, Y.Y. (2010). The use of wearable inertial motion sensors in human lower limb biomechanics studies: A systematic review. *Sensors*, 10(12), 11556–11565. doi:10.3390/s101211556.

Grand, E.L. and Thrun, S. (2012). 3-axis magnetic field mapping and fusion for indoor localization. In *2012 IEEE International Conference on Multisensor Fusion and Integration for Intelligent Systems (MFI)*, 358–364. doi:10.1109/MFI.2012.6343024.

Kok, M., Hol, J.D., and Schön, T.B. (2014). An optimization-based approach to human body motion capture using inertial sensors. *IFAC Proceedings Volumes*, 47(3), 79–85. doi:10.3182/20140824-6-ZA-1003.02252.

Laidig, D., Schauer, T., and Seel, T. (2017a). Exploiting kinematic constraints to compensate magnetic disturbances when calculating joint angles of approximate hinge joints from orientation estimates of inertial sensors. In *2017 International Conference on Rehabilitation Robotics (ICORR)*, 971–976. doi:10.1109/ICORR.2017.8009375.

Laidig, D., Lehmann, D., Bégin, M.A., and Seel, T. (2019). Magnetometer-free realtime inertial motion tracking by exploitation of kinematic constraints in 2-dof joints. *2019 41st Annual International Conference of the IEEE Engineering in Medicine and Biology Society (EMBC)*, 1233–1238.

Laidig, D., Müller, P., and Seel, T. (2017b). Automatic anatomical calibration for imu-based elbow angle measurement in disturbed magnetic fields. *Current Directions in Biomedical Engineering*, 3(2).

Miller, N., Jenkins, O.C., Kallmann, M., and Mataric, M.J. (2004). Motion capture from inertial sensing for untethered humanoid teleoperation. In *4th IEEE/RAS International Conference on Humanoid Robots, 2004.*, volume 2, 547–565 Vol. 2. doi:10.1109/ICHR.2004.1442670.

Olsson, F., Seel, T., Lehmann, D., and Halvorsen, K. (2019). Joint axis estimation for fast and slow movements using weighted gyroscope and acceleration constraints. In *2019 22th International Conference on Information Fusion (FUSION)*, 1–8.

Salchow-Hömmen, C., Callies, L., Laidig, D., Valtin, M., Schauer, T., and Seel, T. (2019). A tangible solution for hand motion tracking in clinical applications. *Sensors*, 19(1), 208. doi:10.3390/s19010208.

Seel, T., Graurock, D., and Schauer, T. (2015). Realtime assessment of foot orientation by accelerometers and gyroscopes. *Current Directions in Biomedical Engineering*, 1(1).

Seel, T., Raisch, J., and Schauer, T. (2014). IMU-based joint angle measurement for gait analysis. *Sensors*, 14(4), 6891–6909. doi:10.3390/s140406891.

Seel, T. and Ruppin, S. (2017). Eliminating the effect of magnetic disturbances on the inclination estimates of inertial sensors. *IFAC-PapersOnLine*, 50(1), 8798–8803. doi:10.1016/j.ifacol.2017.08.1534.

Shu, Y., Bo, C., Shen, G., Zhao, C., Li, L., and Zhao, F. (2015). Magicol: Indoor localization using pervasive magnetic field and opportunistic WiFi sensing. *IEEE Journal on Selected Areas in Communications*, 33(7), 1443–1457. doi:10.1109/JSAC.2015.2430274.

Subbu, K.P., Gozick, B., and Dantu, R. (2013). LocateMe: Magnetic-fields-based indoor localization using smartphones. *ACM Trans. Intell. Syst. Technol.*, 4(4), 73:1–73:27. doi:10.1145/2508037.2508054.

Taetz, B., Bleser, G., and Miezal, M. (2016). Towards self-calibrating inertial body motion capture. In *2016 19th International Conference on Information Fusion (FUSION)*, 1751–1759.

Wenk, F. and Frese, U. (2015). Posture from motion. In *2015 IEEE/RSJ International Conference on Intelligent Robots and Systems (IROS)*, 280–285. doi:10.1109/IROS.2015.7353386.

Wong, C., Zhang, Z., Lo, B., and Yang, G. (2015). Wearable sensing for solid biomechanics: A review. *IEEE Sensors Journal*, 15(5), 2747–2760. doi:10.1109/JSEN.2015.2393883.